Cement and Concrete Research 40 (2010) 731–739

Contents lists available at ScienceDirect

Cement and Concrete Research

journal homepage: http://ees.elsevier.com/CEMCON/default.asp

# Micrometer-scale 3-D shape characterization of eight cements: Particle shape and cement chemistry, and the effect of particle shape on laser diffraction particle size measurement

S.T. Erdoğan [a], X. Nie [b], P.E. Stutzman [c], E.J. Garboczi [c,*]

[a] Middle East Technical University, Dept. of Civil Engineering, Ankara 06531, Turkey
[b] Johns Hopkins University, Department of Physics, Baltimore, Maryland, USA
[c] Inorganic Materials Group, Materials and Construction Research Division, Building and Fire Research Laboratory, National Institute of Standards and Technology, Gaithersburg, Maryland, USA

ARTICLE INFO

*Article history:*
Received 21 December 2007
Accepted 17 December 2009

*Keywords:*
A. Fineness, grinding
B. Characterization, particle size distribution, laser diffraction
E. Cement manufacturers

ABSTRACT

Eight different portland cements were imaged on a synchrotron beam line at Brookhaven National Laboratory using X-ray microcomputed tomography at a voxel size of about 1 μm per cubic voxel edge. The particles ranged in size roughly between 10 μm and 100 μm. The shape and size of individual particles were computationally analyzed using spherical harmonic analysis. The particle shape difference between cements was small but significant, as judged by several different quantitative shape measures, including the particle length, width, and thickness distributions. It was found that the average shape of cement particles was closely correlated with the volume fraction of $C_3S$ (alite) and $C_2S$ (belite) making up the cement powder. It is shown that the non-spherical particle shape of the cements strongly influence laser diffraction results, at least in the sieve size range of 20 μm to 38 μm. Since laser diffraction particle size measurement is being increasingly used by the cement industry, while cement chemistry is always a main factor in cement production, these results could have important implications for how this kind of particle size measurement should be understood and used in the cement industry.

Published by Elsevier Ltd.

## 1. Introduction

Concrete, mortar, and cement paste are composite materials, made up of particulate inclusions in a fluid (before set) or solid (after set) matrix phase. Mortar and concrete have sand and gravel as the inclusions and cement paste is the matrix. The shape of the sand and gravel particles can strongly influence overall properties like fresh concrete viscosity and hardened concrete elastic moduli, water permeability, ionic diffusivity, and compressive and tensile strength [1–4]. The cement and concrete technical community tries to quantify sand and gravel shape via standards like ASTM D4791, in which the length, width, and thickness of an aggregate are measured [5].

In the case of cement paste, before setting the inclusions are multi-phase cement particles, and the matrix phase is water. Of course, dissolution and reaction over time greatly alter the shape of the original particles as they hydrate to form a solid matrix. But at early curing ages, the shape of the particles has a large influence on particle dissolution (via particle surface curvature), chemical reactions (via particle surface area to volume ratio), and early-age mechanical properties (via the overall particle shape). Since the cement particles are fragments ground from larger clinker particles, one might ask if particle shape is related at all to the average composition of cement particles, which can be obtained from quantitative scanning electron microscopy [6].

Three dimensional cement particle shape is not, at present, quantified by any existing standard. However, size determination of powders is a well-developed field [7], with the most common technique being laser diffraction (LD) (general principles are in Ref. [7]), which is also increasingly being used for characterizing cement powders [8]. The effect of particle shape is not usually explicitly considered in LD particle size instruments, but this topic has been considered extensively in the LD particle analyzer literature [7,9–17].

Commonly, the "size" of a particle is given in terms of some kind of "equivalent spherical diameter." That is, a sphere and its diameter are defined so that some geometrical attribute is equivalent to that of the real particle. One concept is the volume equivalent spherical diameter (VESD), where the volume of the sphere is chosen to be equal to that of the real particle. Laser diffraction software computes effective spherical diameters based on the measured diffraction pattern as perceived by detector geometry [12–15]. Results can also depend on non-spherical particle alignment in the suspending fluid [12–15].

* Corresponding author.
*E-mail address:* edward.garboczi@nist.gov (E.J. Garboczi).

0008-8846/$ – see front matter. Published by Elsevier Ltd.
doi:10.1016/j.cemconres.2009.12.006

Recent work has shown quantitatively, for microfine aggregate particles (particles passing a 75 μm sieve), that laser diffraction size results are different from some other "size" results for non-fibrous randomly-shaped particles [17]. The edge length of a square sieve opening is another choice for an effective "size," as well as other possibilities available if one has the data to go beyond single-parameter effective shapes [18].

X-ray computed tomography (CT) is a technique that can measure 3-D microstructure with voxel sizes well below one micrometer, though a voxel size of 1–2 μm is more common [19]. This technique is being increasingly used in the field of cement and concrete to quantitatively visualize 3-D structure and microstructure [20–23]. It can also be used to measure 3-D particle shape by scanning a dilute suspension of particles [17,18,24,25] and analyzing the 3-D images obtained with spherical harmonics techniques [24]. Spherical harmonic analysis of particle shape has also been applied in the medical field to assess tumor shape [26]. This technique has been initially applied to cement particle shape [27] using particle images from Ref. [23].

The purpose of this paper is to present 3-D shape results for eight different cements and relate these results for cement chemistry and to laser diffraction particle size distribution (psd) results. X-ray micro-computed tomography at a synchrotron beam line at Brookhaven National Laboratory was used to image the cement particles at a voxel size of about 1 μm per cubic voxel edge. Laser diffraction particle size data from a commercial instrument was also obtained, along with quantitative mineral composition in 2-D using a scanning electron microscope and X-ray microprobe. Both 3-D qualitative images and 3-D quantitative shape analysis from X-ray CT will be presented below. It will be shown that the cement chemistry or mineralogy appears to affect the particle shape, and that the non-spherical particle shape of the cements influences the laser diffraction results, at least in the sieve size range of 20 μm to 38 μm. These results have implications for how laser diffraction psd curves of cement powders should be understood and used in the cement industry.

## 2. Materials

The mineralogical analysis of the eight cements studied was carried out by scanning electron microscope characterization using backscattered electron (BE) and X-ray (XR) imaging and quantitative X-ray diffraction [6,28,29]. Table 1 provides either a NIST internal label (MA prefix), or the number of the Cement and Concrete Reference Laboratory (CCRL, www.ccrl.us) proficiency cement used, along with the ASTM cement type designation and the volume fraction of clinker phases. Refs. [6,28,29] have details of the experimental uncertainties — a rough value is 1% to 2% in each value listed in Table 1. The amount of calcium sulfate in each cement, and the forms of calcium sulfate present, were characterized by X-ray powder diffraction but are not presented here. The cement types include ASTM Type 1, Type V, and a white cement.

**Table 1**
Mineralogical analysis of each cement (volume fraction).

| Cement name | Type | $C_3S$ (alite) | $C_2S$ (belite) | $C_3A$ (aluminate) | $C_4AF$ (ferrite) |
|---|---|---|---|---|---|
| CCRL 116 | ASTM Type I | 0.6708 | 0.2217 | 0.0711 | 0.0364 |
| CCRL 140 | ASTM Type I | 0.6576 | 0.1800 | 0.0994 | 0.0633 |
| MA 165 | ASTM Type V | 0.6885 | 0.1775 | 0.0313 | 0.1027 |
| MA 178 | White | 0.6704 | 0.2554 | 0.0731 | 0.0000 |
| CCRL 141 | ASTM Type I | 0.6826 | 0.1147 | 0.1237 | 0.0790 |
| CCRL 152 | ASTM Type I | 0.7343 | 0.0938 | 0.1311 | 0.0407 |
| MA 157 | ASTM Type I | 0.6652 | 0.1710 | 0.0988 | 0.0650 |
| MA 160 | ASTM Type I | 0.5213 | 0.3612 | 0.0507 | 0.0668 |

## 3. Particle shape experimental techniques

Sieving was used to narrow the range of particle sizes examined, followed by psd measurement via laser diffraction and particle shape/volume determination via X-ray CT.

### 3.1. Sieve analysis

To prepare the cements for the laser diffraction experiments, the cements were first sieved between the 20 μm and 38 μm sieves. The sieves were used on a microclassifying unit, with the application of extended doses of ultrasound and long sieving times used with both sieves to make sure that sieving was essentially complete. For preparing the cements for the X-ray μCT experiments, the upper sieve was not used. Therefore, only particles with nominal size greater than 20 μm were used in the X-ray CT measurements. The maximum size particle seen in the X-ray CT scans had a VESD of about 60 μm, so the particle size range studied in the X-ray CT scans was about 20 μm to 60 μm. Although there can be systematic particle shape changes with particle size, from previous studies any particle shape changes should be negligible over this small range [30].

### 3.2. Laser diffraction particle size distribution

Scattering of light from particles is due to differences between the refractive indices of the particles and the medium containing the particles. The complex refractive index of a material, $n+ik$ (where $n$ is the real part and $k$ the imaginary part), must be known in order to be able to calculate the psd of a powder sample of this material using the Mie theory [31,32], which assumes spherical particles. Mie theory takes into account absorption, and so requires knowledge of the complex refractive index. For cement, the imaginary part of the refractive index is not well known for each cement phase, and the method of averaging these values for multi-phase particles, for both $n$ and $k$, has not been well-established. The value of $k$ used when employing Mie theory to interpret LD measurements does affect the measurements at particles less than a few micrometers in size [8]. For particles larger than about 5 times to 40 times the wavelength of the incident light, the Fraunhofer approximation [31], which only considers forward scattering and does not use the value of $k$, can be used to determine the psd. The LD particle size analyzer used in this study had a laser wavelength of 650 nm, and the smallest particle had a size of about 20 μm, so that the ratio of particle size to light wavelength was about 30 at the minimum. The same LD results were found whether using Mie or Fraunhofer theory to interpret the results, as expected.

For portland cement, suspending the particles in isopropyl alcohol has been found to give reproducible results [8]. In this case, the particles are suspended in the alcohol and circulate through a broadened beam of laser light. The particles scatter the incident light onto a lens, which focuses the scattered light onto a detector array. The psd is calculated via inverting an integral equation constructed from the collected diffracted light data [33]. It takes about 20 min to obtain a valid, reproducible LD psd [8]. The spherical particle assumption made in LD is particularly important. The reproducibility of LD results for cement powders depends mostly on sampling practices, and is quite high, about 1% or better for the same sample [8], similar to other powdered materials [34].

### 3.3. X-ray CT

Details about the X-ray CT sample preparation were given elsewhere [17,25]. Briefly, the sieved cement was mixed with epoxy and the resulting mixture inserted into small plastic cylinders of diameter 1 mm to 2 mm. The amount of particles in the mixture did not exceed a volume fraction of about 15%. The heights of the

specimens were 20 mm to 60 mm; however, the actual part of the specimen scanned was often less than 2 mm in extent. Sample preparation was about an hour plus epoxy hardening time for each cement. X-ray CT scanning time and image reconstruction was about 4 h for each cement, and the computational and mathematical analysis to obtain individual particle and particle quantities took up to 12 h per cement. The additional time for presenting the data in various formats was negligible.

In the X-ray CT technique, X-rays penetrate a 3-D sample at many different angles and the absorption is measured. A computer-based reconstruction technique then makes gray level images, where each image is a slice of the sample and the contrast in gray levels is caused by the different X-ray absorption properties of the materials in the sample [35,36]. When these 2-D images are stacked together, a 3-D view of the sample interior is obtained, which is thresholded to produce the final cement particle image. Individual particles are computationally extracted from this large image. A cubic voxel size of edge length about 1 μm was used for the CT results presented in this paper. This kind of X-ray CT data has been shown to give individual particle volumes accurate to about 1% to 2% [18].

## 4. Mathematical and computational techniques

Any 3-D voxel particle data can be used to generate spherical harmonic (SH) functions [24], which are then employed to create a smooth approximation to the function $r(\theta,\phi)$, which is the distance from the center of volume to the particle surface in the direction given by the spherical polar angles $(\theta,\phi)$. Using this analytical function, one can compute any geometric quantity of the particle like volume, surface area, or moment of inertia [18,24,37] that depends on surface or volume integrals, and one can also generate 3-D images in various formats. Fig. 1 shows an original particle as obtained from the X-ray microCT, in terms of a collection of voxels (left), and the right image shows the particle as reconstructed using the spherical harmonic coefficients and shown in VRML (virtual reality modeling language) mode [25]. The two particle representations shown in Fig. 1 are not identically oriented, but have only been roughly aligned by eye. Building a particle out of spherical harmonic coefficients tends to smooth the "digital roughness" of the original experimental image.

Another computation that does not depend on surface or volume integrals is the length–width–thickness computation for each particle (ASTM D4791) [5,18]. The length ($L$) is defined as the largest straight-line surface-to-surface distance on the particle. The width ($W$) is defined similarly, except that it must be perpendicular to the length. The thickness ($T$) is also defined similarly, except that it must be perpendicular to both the length and the width. This is a well-defined and unique way, in 3-D, to obtain three orthogonal lengths from an irregular body. Note that this procedure does not depend on the assumption of any kind of an equivalent regular shape. These values are well defined and unique for each particle, but of course these three measures do not necessarily represent the random particle shape as a whole.

## 5. Results

### 5.1. Particle shape analysis

The X-ray microCT results are first presented qualitatively in Fig. 2 by showing images of a typical particle for each kind of cement. One sees that the particles are definitely not well-represented by spheres, and that the particle shapes appear to be random. Table 2 lists how many valid [25] particles were actually found for each cement. Enough particles of each cement were found so that reasonable particle statistics could be obtained.

The $L$, $W$, and $T$ results were computed for each cement, and the $L$ and $W$ results were normalized, for each particle, by the value of $T$ ($\mathtt{L}\equiv L/T$ and $\mathtt{W}\equiv W/T$). Table 2 lists the average value of L, W, and the average of the quantity $\mathtt{L/W}=L/W$ taken over all the particles for a given cement. The "uncertainty" values in the table are simply the standard deviation of the quantity, which gives a measure of how widely these values are spread across the particles of a given cement type. The quantity L/W is one kind of aspect ratio for the particle, and gives some indication of its non-sphericity. Since these particles have random shapes, one can form many kinds of aspect ratios from many different definitions of dimensions [18].

By studying how these average values changed as subsets of the data were used, it is believed that having a larger number of particle images available would not have changed these average values significantly. The average values of L ranged from 1.79 to 2.33, while the average values of W ranged from a low of 1.40 to a high of 1.67. The range of the average value of the ratio, L/W, was 1.28 to 1.42. It is interesting to note that the cement with the lowest average value of L/W, MA 160, had the largest volume fraction of $C_2S$ (belite) and the lowest volume fraction of $C_3S$ (alite). Similarly, the cement with the highest average value of L/W, CCRL152, had the lowest volume fraction of $C_2S$ (belite) and the highest volume fraction of $C_3S$ (alite).

Fig. 3 shows the average values of L/W for each cement plotted vs. the amounts of $C_2S$ (belite) and $C_3S$ (alite) measured in each cement. It is clear that increasing the amount of $C_3S$ (alite) tends to increase the aspect ratio of all the cements, while increasing the amount of $C_2S$ (belite) has the opposite effect. Note that all the cements were produced in a ball-mill grinding process, so experienced similar mechanics. The last column in Table 2 will be discussed later below.

The shape distribution for each kind of particle can be seen by examining the 2-D L–W histogram for each particle, shown in Table 3. The 2-D L–W histogram is simply defined [18]. A given entry in the histogram shows the number fraction, expressed as a percentage, of

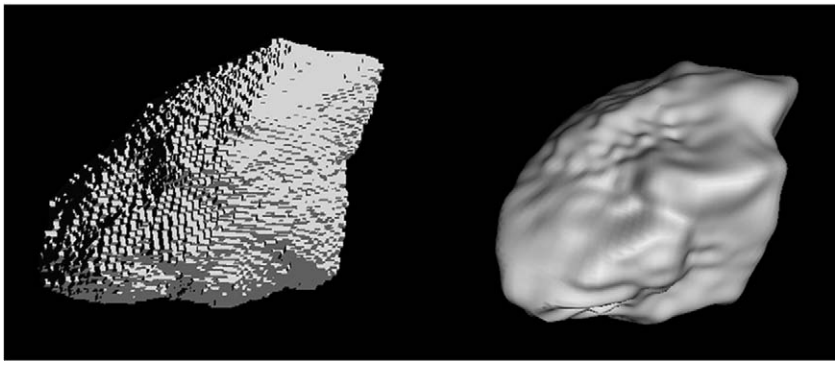

**Fig. 1.** Left — 3-D digital particle extracted and thresholded from the X-ray microCT, right — VRML image of same particle (CCRL 152 cement) reconstructed from its spherical harmonic expansion.

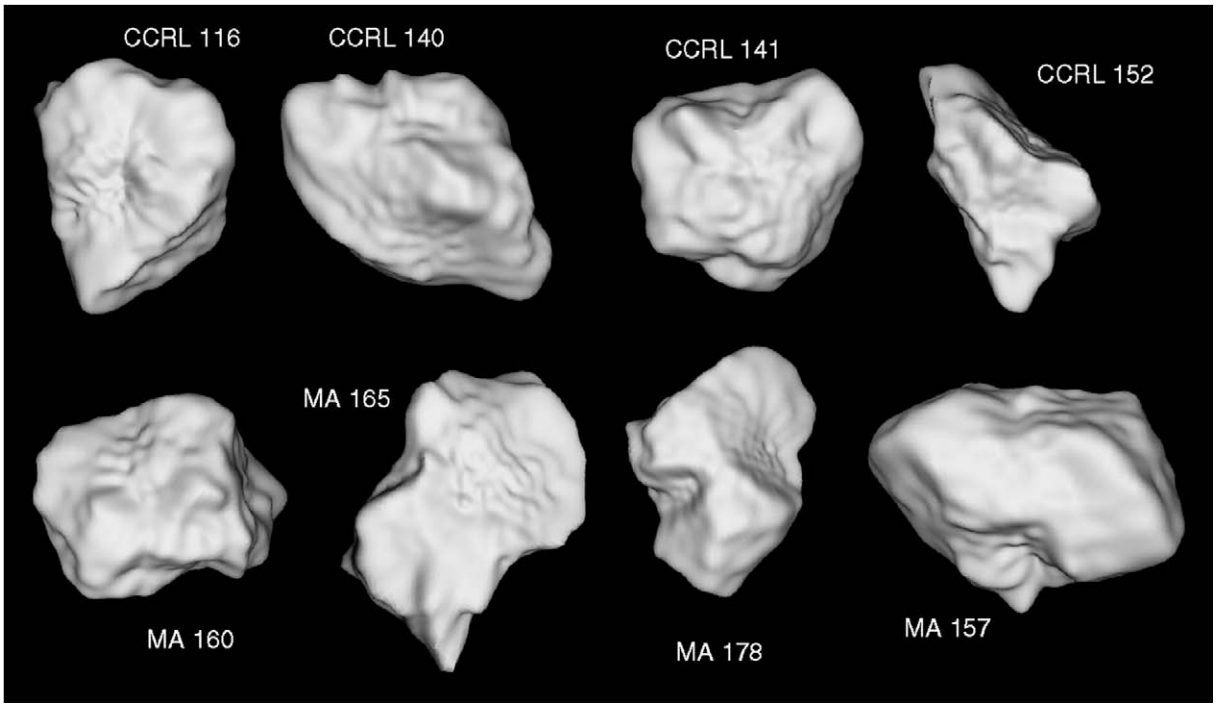


**Fig. 2.** A sampling of the eight different cements, showing the range of particle shapes available (not to scale).

particles whose value of L and whose value of W fall between certain limits. Consider, for example, the gray bins in the CCRL 116 cement entry in Table 3: 16.6% of the CCRL 116 particles have values of L between 1 and 1.5, and values of W between 1 and 1.5, 35.4% have values of L between 1.5 and 2 and values of W between 1 and 1.5, 10.3% have values of L between 1.5 and 2 and values of W between 1.5 and 2, and 0% have values of L between 1 and 1.5 and values of W between 1.5 and 2, since by definition, $W \leq L$.

Consider the last column in Table 2, which gives the sum of the numbers in the gray area of Table 3 for each cement. This sum represents the percentages of all particles that only have modest values of L and W, and so tend to be more equi-axed. Note that cement MA 160 has the highest value of this sum, 75%, and it has the lowest average value of L/W, 1.28. The cement with the lowest value in the last column of Table 2, CCRL 152, also has the highest average value of L/W, 1.42. The higher the value of the average "aspect ratio," L/W, the lower the amount of particles that will appear in the approximately equi-axed (gray-shaded) part of the histogram.

Cements CCRL 116, CCRL 140, MA 165, and MA 178, listed in the top half of Table 3, appear similar to each other in terms of their shape distributions. The sums of the gray areas, as listed in Table 2, are almost the same, and the distribution of the particles across various bins in Table 3 are similar as well. It is interesting to note that these four cements include all three types, ASTM Type I, Type V, and a white cement. Note from Table 1 that these four cements had very similar volume fractions of $C_3S$ and $C_2S$. In the lower half of Table 3, CCRL 141, CCRL 152, and MA 157 are also similar to each other, with less weight in the gray area than the four cements in the top half of the table and consequently higher average values of L/W as given in Table 2.

Fig. 4 plots the sum of the values in the gray areas in Table 3 for each cement vs. the volume fraction of $C_3S$ (left) and the volume fraction of $C_2S$ (right). Again, as in Fig. 3, there is a clear trend with these phases. Increasing the amount of $C_3S$ decreases, roughly linearly, the number fraction of the more equi-axed particles, while increasing the amount of $C_2S$ increases the number fraction of more equi-axed particles.

Since the grinding process reduces clinker nodules (and added gypsum) to cement powder, these differences in shape must arise from grinding, the clinker texture and phase composition, and the different grindability of the constituent phases. While grinding is a complicated process, factors influencing grindability include hardness of the individual phases, internal porosity, crystal size, and defects such as microcracking [38]. In addition, the fracture toughness of each phase as well as each phase's plasticity influences the response to the grinding process. The hardness of the crystal phases have been measured using nanoindentation [39], and have been found to be nearly the same, within experimental uncertainty. Alite exhibits fractures in cement clinker (most likely cooling-related) and ground cement that appear like cleavage planes. Belite crystals have a rounded habit and while they do exhibit good cleavage on the {100} plane [40], do not appear to have a tendency to cleave when ground. Finally, the texture of the matrix phases (ferrite and aluminate) and occurrence and texture of other phases (periclase) may also influence the fracture characteristics of a clinker. These characteristics could help explain the results shown in Fig. 4. Cements with more alite are ground by breaking alite crystals, producing less equi-axed particles. Cements with more belite have less of a tendency to have broken particles, so will have a higher percentage of equi-axed particles. This

**Table 2**
Number of particles analyzed for each cement, along with average normalized dimensions.

| Cement name | Number of particles extracted | Average L | Average W | Average L/W | Sum of gray bins in Table 3 |
|---|---|---|---|---|---|
| CCRL 116 | 3172 | 1.97 ± 0.56 | 1.47 ± 0.35 | 1.35 ± 0.25 | 62.3 |
| CCRL 140 | 3327 | 1.97 ± 0.57 | 1.47 ± 0.34 | 1.34 ± 0.26 | 62.0 |
| MA 165 | 6242 | 1.97 ± 0.54 | 1.46 ± 0.33 | 1.35 ± 0.26 | 60.9 |
| MA 178 | 2662 | 1.99 ± 0.56 | 1.50 ± 0.37 | 1.33 ± 0.24 | 59.9 |
| CCRL 141 | 1593 | 2.21 ± 0.63 | 1.58 ± 0.40 | 1.41 ± 0.30 | 44.3 |
| CCRL 152 | 1108 | 2.33 ± 0.68 | 1.67 ± 0.44 | 1.42 ± 0.30 | 36.0 |
| MA 157 | 1946 | 2.10 ± 0.57 | 1.53 ± 0.35 | 1.39 ± 0.29 | 49.7 |
| MA 160 | 4192 | 1.79 ± 0.48 | 1.40 ± 0.30 | 1.28 ± 0.21 | 75.0 |

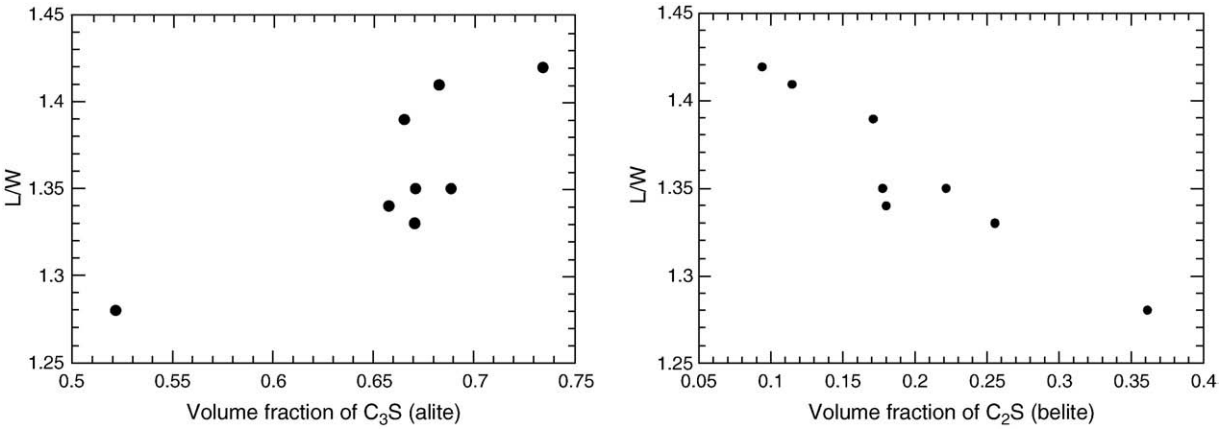


**Fig. 3.** Left — the average value of L/W plotted vs. the volume fraction of $C_3S$ (alite), for the eight cements; (right) the average value of L/W plotted vs. the volume fraction of $C_2S$ (belite), for the eight cements.

is seen in the SEM micrographs in Fig. 5, where cement MA 160 (left side) grains appear more rounded with liberated belite crystals. In contrast, CCRL 152 cement grains (right side) are more angular, including the fractured belite, with fewer liberated belite crystals.

### 5.2. Laser diffraction psd measurement and analysis

Fig. 6 shows the cumulative psd curves, as measured by laser diffraction, for all eight cements. Using cumulative psd curves is a

**Table 3**
2-D L/W histogram for each of the eight kinds of particles. The normalized width, W, is along the vertical axis, and the normalized length, L, is along the horizontal axis. The numbers in the table are number fractions, expressed in percentages.

| CCRL 116 | | | | | | | CCRL 140 | | | | | | |
|---|---|---|---|---|---|---|---|---|---|---|---|---|---|
| 3.5 – 4 | 0 | 0 | 0 | 0 | 0 | 0.0 | 3.5 – 4 | 0 | 0 | 0 | 0 | 0 | 0.0 |
| 3 – 3.5 | 0 | 0 | 0 | 0 | 0.1 | 0.2 | 3 – 3.5 | 0 | 0 | 0 | 0 | 0.0 | 0.1 |
| 2.5 – 3 | 0 | 0 | 0 | 0.4 | 0.5 | 0.4 | 2.5 – 3 | 0 | 0 | 0 | 0.3 | 0.4 | 0.3 |
| 2 – 2.5 | 0 | 0 | 1.7 | 2.3 | 1.2 | 0.4 | 2 – 2.5 | 0 | 0 | 1.7 | 2.8 | 1.2 | 0.5 |
| 1.5 – 2 | 0 | 10.3 | 13.2 | 4.1 | 1.4 | 0.2 | 1.5 – 2 | 0 | 10.0 | 12.7 | 4.4 | 1.4 | 0.3 |
| 1 – 1.5 | 16.6 | 35.4 | 8.6 | 1.4 | 0.6 | 0.0 | 1 – 1.5 | 18.3 | 33.7 | 8.7 | 1.5 | 0.4 | 0.0 |
| W/L | 1 – 1.5 | 1.5 – 2 | 2 – 2.5 | 2.5 – 3 | 3 – 3.5 | 3.5 – 4 | W/L | 1 – 1.5 | 1.5 – 2 | 2 – 2.5 | 2.5 – 3 | 3 – 3.5 | 3.5 – 4 |
| MA 165 | | | | | | | MA 178 | | | | | | |
| 3.5 – 4 | 0 | 0 | 0 | 0 | 0 | 0.0 | 3.5 – 4 | 0 | 0 | 0 | 0 | 0 | 0.1 |
| 3 – 3.5 | 0 | 0 | 0 | 0 | 0.0 | 0.1 | 3 – 3.5 | 0 | 0 | 0 | 0 | 0.0 | 0.2 |
| 2.5 – 3 | 0 | 0 | 0 | 0.3 | 0.4 | 0.2 | 2.5 – 3 | 0 | 0 | 0 | 0.4 | 0.7 | 0.5 |
| 2 – 2.5 | 0 | 0 | 1.7 | 2.3 | 1.3 | 0.5 | 2 – 2.5 | 0 | 0 | 2.1 | 3.2 | 1.7 | 0.5 |
| 1.5 – 2 | 0 | 9.8 | 13.2 | 4.3 | 1.2 | 0.4 | 1.5 – 2 | 0 | 9.2 | 13.1 | 5.2 | 1.2 | 0.4 |
| 1 – 1.5 | 17.7 | 33.4 | 9.9 | 2.0 | 0.2 | 0.1 | 1 – 1.5 | 19.1 | 31.6 | 8.4 | 1.2 | 0.3 | 0.0 |
| W/L | 1 – 1.5 | 1.5 – 2 | 2 – 2.5 | 2.5 – 3 | 3 – 3.5 | 3.5 – 4 | W/L | 1 – 1.5 | 1.5 – 2 | 2 – 2.5 | 2.5 – 3 | 3 – 3.5 | 3.5 – 4 |

| CCRL 141 | | | | | | | CCRL 152 | | | | | | |
|---|---|---|---|---|---|---|---|---|---|---|---|---|---|
| 3.5 – 4 | 0 | 0 | 0 | 0 | 0 | 0.0 | 3.5 – 4 | 0 | 0 | 0 | 0 | 0 | 0.0 |
| 3 – 3.5 | 0 | 0 | 0 | 0 | 0.2 | 0.4 | 3 – 3.5 | 0 | 0 | 0 | 0 | 0.1 | 0.3 |
| 2.5 – 3 | 0 | 0 | 0 | 1.1 | 0.9 | 0.7 | 2.5 – 3 | 0 | 0 | 0 | 0.5 | 2.2 | 0.8 |
| 2 – 2.5 | 0 | 0 | 2.6 | 3.9 | 1.8 | 1.2 | 2 – 2.5 | 0 | 0 | 3.3 | 7.1 | 3.7 | 1.5 |
| 1.5 – 2 | 0 | 8.8 | 16.3 | 6.2 | 2.6 | 0.6 | 1.5 – 2 | 0 | 8.2 | 17.6 | 6.9 | 2.6 | 0.9 |
| 1 – 1.5 | 8.0 | 27.5 | 10.9 | 3.2 | 0.8 | 0.3 | 1 – 1.5 | 7.0 | 20.8 | 9.6 | 2.8 | 0.7 | 0.5 |
| W/L | 1 – 1.5 | 1.5 – 2 | 2 – 2.5 | 2.5 – 3 | 3 – 3.5 | 3.5 – 4 | W/L | 1 – 1.5 | 1.5 – 2 | 2 – 2.5 | 2.5 – 3 | 3 – 3.5 | 3.5 – 4 |
| MA 157 | | | | | | | MA 160 | | | | | | |
| 3.5 – 4 | 0 | 0 | 0 | 0 | 0 | 0.0 | 3.5 – 4 | 0 | 0 | 0 | 0 | 0 | 0.0 |
| 3 – 3.5 | 0 | 0 | 0 | 0 | 0.1 | 0.2 | 3 – 3.5 | 0 | 0 | 0 | 0 | 0.0 | 0.0 |
| 2.5 – 3 | 0 | 0 | 0 | 0.4 | 0.5 | 0.5 | 2.5 – 3 | 0 | 0 | 0 | 0.2 | 0.2 | 0.2 |
| 2 – 2.5 | 0 | 0 | 2.4 | 3.3 | 1.9 | 0.6 | 2 – 2.5 | 0 | 0 | 1.4 | 1.8 | 0.6 | 0.3 |
| 1.5 – 2 | 0 | 9.5 | 16.1 | 6.0 | 1.5 | 0.3 | 1.5 – 2 | 0 | 9.6 | 9.5 | 2.5 | 1.0 | 0.1 |
| 1 – 1.5 | 11.1 | 29.1 | 11.4 | 2.7 | 0.7 | 0.3 | 1 – 1.5 | 28.6 | 36.8 | 5.5 | 0.9 | 0.1 | 0.0 |
| W/L | 1 – 1.5 | 1.5 – 2 | 2 – 2.5 | 2.5 – 3 | 3 – 3.5 | 3.5 – 4 | W/L | 1 – 1.5 | 1.5 – 2 | 2 – 2.5 | 2.5 – 3 | 3 – 3.5 | 3.5 – 4 |

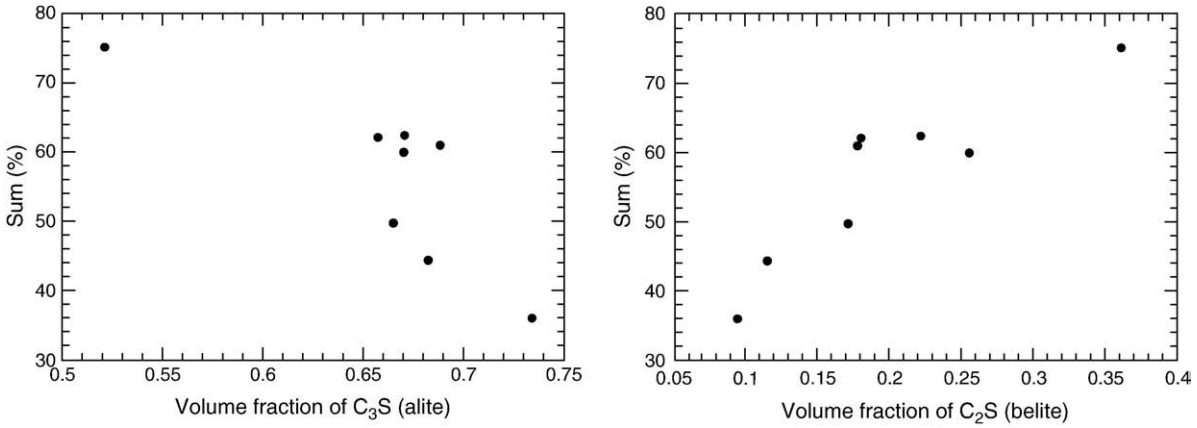


**Fig. 4.** The last column of Table 2, which contains the sum of the gray areas in Table 3, plotted vs. the $C_3S$ (alite) volume fraction (left) and vs. the $C_2S$ (belite) volume fraction (right).

simpler and better way to compare psd curves [41] and will be used in the rest of this paper. There are several key pieces of information to be gleaned from Fig. 6. First, all the distributions are qualitatively similar. There are, however, quantifiable differences, as discussed below, which depend on shape differences among the cements.

Secondly, one must remember that all the cements studied, before laser diffraction measurement, were very carefully sieved between 20 μm and 38 μm sieves. Naively, one would say that there should not be particles outside of these sizes showing in Fig. 6. However, the horizontal range of Fig. 6 runs between 15 μm and 80 μm, and one can see that about 35% of the total particle volume lies in a size range beyond 38 μm.

One qualitative explanation of this observation can be obtained by considering the non-sphericity of the particles. Consider a particle with length $L$, width $W$, and thickness $T$. If we think of the particle as passing through a sieve with $L$ out of the plane and $W$ and $T$ in the plane of the sieve, then the particle can pass through a sieve with opening of dimension $W$, even though $L \geq W$ [42–44]. There is also probably a degree of alignment of the particles, since they are non-spherical, in the flow field in the instrument as the particles are carried past the laser in the suspending isopropyl alcohol. However, the statistics of alignment for randomly-shaped particles are not as well-known as they are for simple ellipsoidal particles (Ref. [45] and references therein). This alignment would also tend to broaden the LD curve by extending the results to the maximum $L$ and minimum $T$ values [14,15,17]. But even if there were no alignment, but the particles were randomly arranged, there would still be a similar kind of broadening [9–11,16,17], but the details of the curves between the lower and upper limits would be different. In fact, Ref. [11] says "In reality, the LD psd data, even for mono-sized non-spherical test samples, are a combination of particle breadth, longest dimension, and eventually other particle dimensional measurements for more complex shapes." Detector geometry also affects the detailed aspects of the curves [12,13].

Fig. 7 shows the LD cumulative psd curves, taken from Fig. 6, of the two cements that had the greatest discrepancy in the last column of Table 2, MA160 and CCRL 152. Note that the curve for CCRL 152 extends to larger sizes than that for MA 160, while the two curves have about the same lower size limit. A cumulative psd curve was computed from the X-ray CT results, using the measured VESD of each particle as the "size" on the abscissa and the measured particle volume on the ordinate, is displayed in Fig. 7. Only particles that had $W$

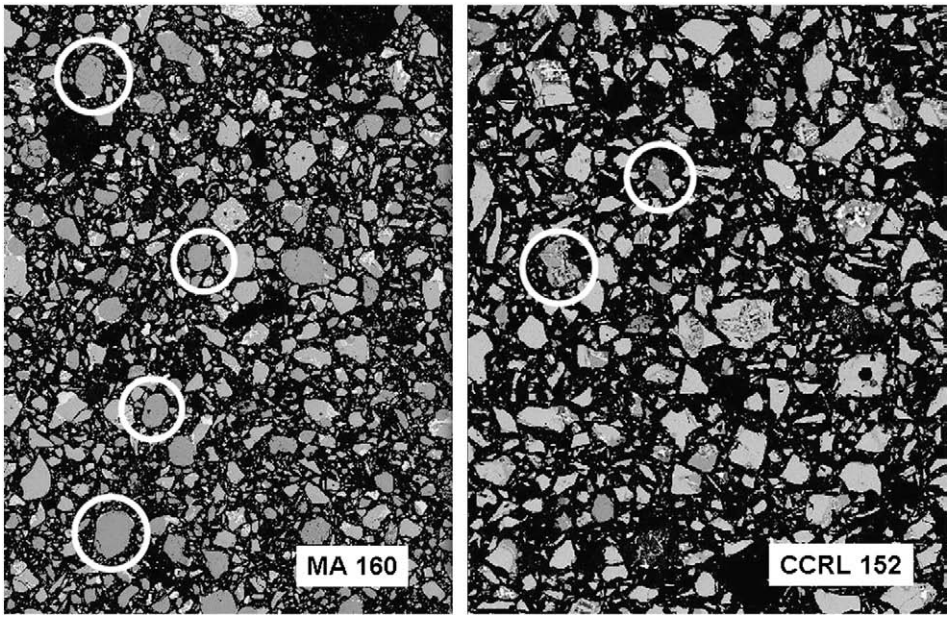


**Fig. 5.** SEM backscattered electron image of polished sections from cements MA 160 (left) and CCRL 152 (right) illustrates the difference in particle angularity. Belite grains (circled, intermediate gray) in MA160 appear to have been liberated from the matrix. In the CCRL 152 cement, they appear to exhibit cross-grain fracture.

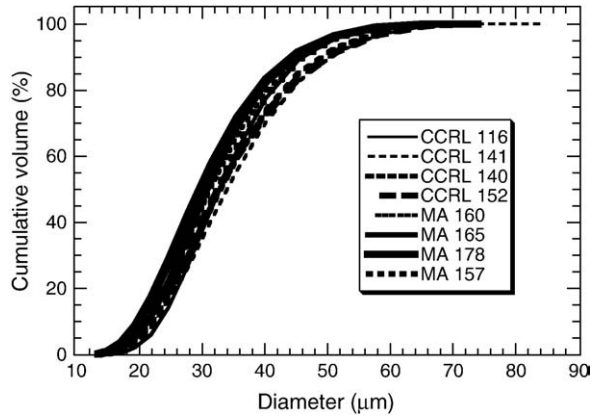


**Fig. 6.** Laser diffraction particle size distributions for all eight cements, in terms of cumulative volume (%) plotted vs. the equivalent spherical diameter as measured by laser diffraction.

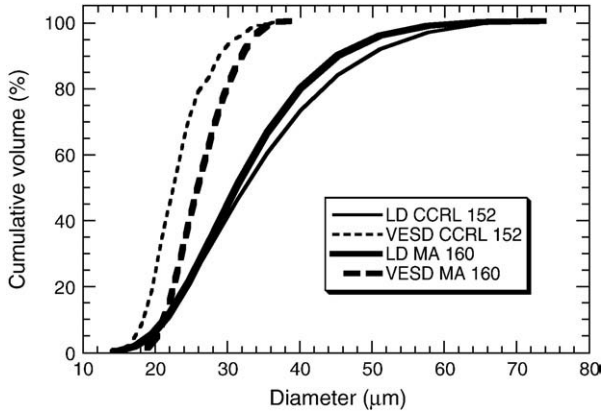


**Fig. 7.** LD psd curves for CCRL 152 and MA 160, in terms of volume fraction and equivalent spherical diameter as measured by laser diffraction, along with psd as measured by X-ray CT, in terms of cumulative volume (%) plotted against the volume equivalent spherical diameter (VESD) as measured by X-ray CT.

between 20 μm and 38 μm as measured by X-ray CT were used in this computation, so as to approximately match the sieving. The volume of particles with VESD less than a given value was computed, and then divided by the total volume of measured particles to generate these psd curves. The volume fraction was expressed as a percentage [41]. Fig. 7 clearly demonstrates that, for these two cements, the VESD is not the same as the equivalent spherical size determined by laser scattering [17], which is also true for other kinds of particles [9,11,14,15,17].

A typical psd curve plots some measure of size on the *x*-axis, and the volume or number fraction of particles on the *y*-axis. To attempt to gain some insight into how the LD results are affected by *"other particle dimensional measurements for more complex shapes"* [11], we construct psd curves using other particle dimensions like *L*, *W*, and *T*. Since these parameters span the size of the particles, in some sense, psd curves constructed using these parameters should be able to also span the LD curves. This is a similar procedure to that proposed in Ref. [11], where 2-D information about shape was used to help determine or fit the LD curves. The X-ray CT data, however, give 3-D information about shape, so should potentially be a better source of shape data with which to interpret LD data.

Fig. 8 shows this kind of analysis for CCRL 152 and MA 160, since they were the two most different cements in terms of shape distributions. In Fig. 8, for each cement, the *L*, *W*, and *T* curves were constructed only from particles that had 20 μm$<W<$38 μm as measured by X-ray μCT. These curves were constructed in a similar fashion to the VESD curves in Fig. 7, but using *L*, *W*, or *T* as the abscissa. In both graphs in Fig. 8, the *W* curve covers the middle part of the LD curve. The *L* curves are shifted to the right, to higher abscissa values, and the *T* curves are shifted to the left, to lower abscissa values. It is interesting to note that the *L* curves tend to match up with the LD curves at the largest sizes. So it seems reasonable to say that the tail of the LD psd curves at higher abscissa values is due to the extent of the length distributions of the real particles.

The *T* curves, however, definitely extend well to the left of the LD curves. This could be an indication of anisotropy in the particle orientations, so that the LD instrument is not picking up the smaller dimensions of the particles. It is known that when anisotropic particles are randomly oriented, the extent of the LD curves essentially go from the smallest to the largest particle dimensions [9–11,14–16].

In Fig. 8, the psd curves that used *L*, *W*, or *T* as the characteristic "size" of a particle appeared to span the laser diffraction curve. Since we can think of the laser as sampling the different size dimensions of the particles, it was of interest to simply add each *L*, *W*, and *T* curve together and divide by three. Again, this is a similar procedure to that proposed in Ref. [11], where information about shape is used to "fit" the LD curves. Fig. 9 shows the results of this process. For both cements, it appears that this approximate curve roughly matches the LD curve, again indicating that the breadth of the LD curve is roughly that of the smallest to largest dimensions of the anisotropic particles. In the CCRL 152 cement graph, the shape of the LWT cumulative psd curve is very similar to that of the LD curve, but is displaced approximate 8 μm to the left. In the MA 160 cement graph, the two

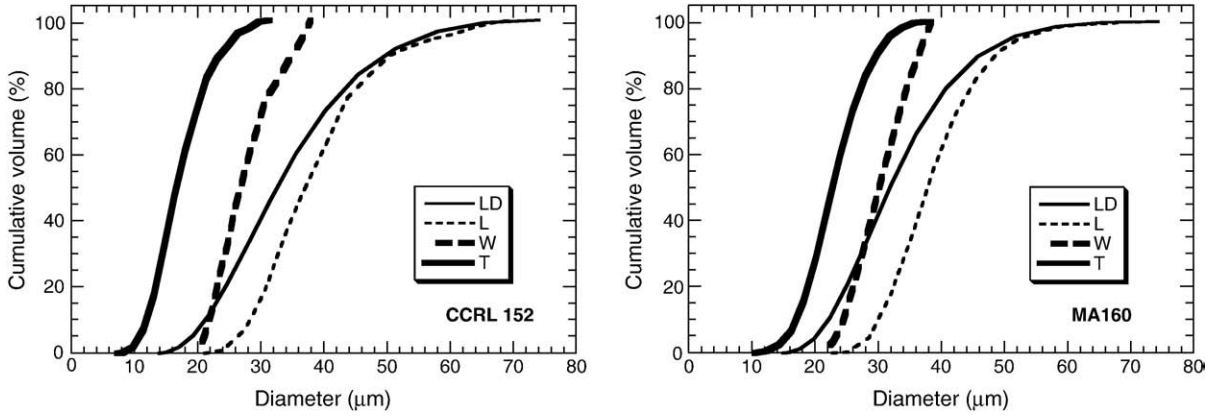


**Fig. 8.** LD psd curves, along with the equivalent psd curves computed from X-ray CT plotted against length, width, and thickness as calculated from the spherical harmonic expansions, for two of the eight cements studied.

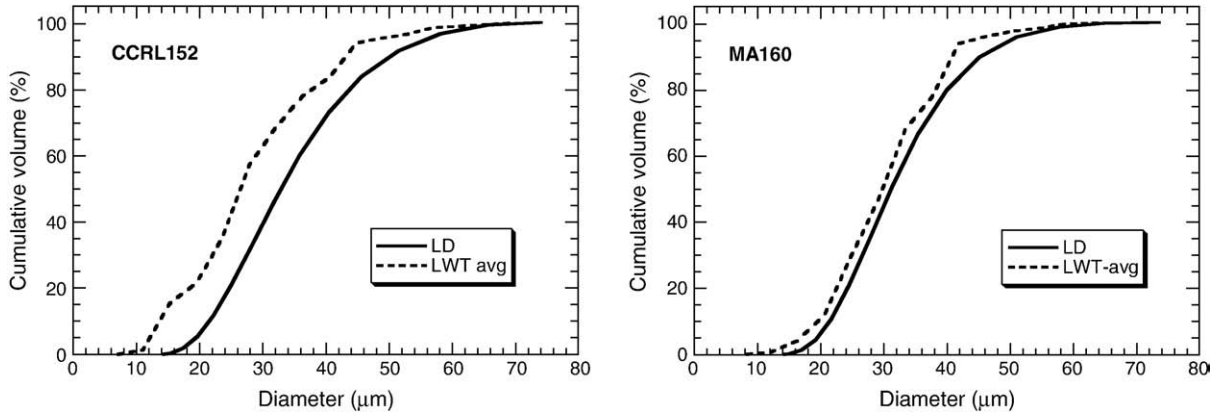


**Fig. 9.** Laser diffraction particle size distributions, along with the equally-weighted average of the psd curves computed from X-ray CT and plotted against the full range of length, width, and thickness as calculated from the spherical harmonic expansions, for two of the eight cements studied.

psd curves lie nearly on top of each other but the LWT curve is still displaced slightly to the left of the LD curve.

## 6. Conclusions

The X-ray microcomputed tomography technique, coupled with spherical harmonic analysis, is useful for quantitatively determining the 3-D shape of cement particles. This information can then be successfully used to analyze other particle size determination methods like laser diffraction and particle sieve analysis by constructing psd curves using the measured volume data and any size that can be defined from the particle geometry. One needs to choose the size that best suits one's purpose in characterizing the particles. It is important to remember that particle size and particle shape are not independent of each other, at least not in most measurement techniques.

For the eight cements studied in this paper, particle shape, at the length scale of 20 μm to about 60 μm, does seem to depend on mineralogy. The amount of $C_3S$ (alite) and $C_2S$ (belite) influenced how equi-axed the particles tended to be. Cements with higher amounts of belite tended to have more equi-axed shapes than did cements with lower amounts of belite and thus higher amounts of alite. Additional analysis is needed to better define this relationship. The cements were of three types: ASTM Type I, Type V, and a white cement. The cement type did not seem to exhibit any relationship to the particle shape differences; only the general cement composition seemed relevant.

Finally, it is important to note the effect that non-spherical particle shape has on laser diffraction psd curves. When one refers to the "diameter" of the particles as found by laser diffraction, one is not referring to the volume equivalent spherical diameter (VESD) but only some equivalent scattering diameter that is a function of the particle geometry distribution, any particle alignment in the suspending fluid in the LD device, and the laser light detector geometry. For the eight cements studied in this paper, these two equivalent spherical diameters were indeed quite different. Because of these effects, those cement plants that are using laser diffraction for automatic process control and those who are designing experiments that use cement size as a variable, say in a reactivity or set time experiment, need to be aware of the fact that the actual cement particle sizes/volumes will tend to be somewhat smaller than what is measured in LD.

## 7. Future research needs

Now that we can quantitatively characterize the shape of random particles, and therefore use them in any quantitative calculation, we need to calculate the actual scattering that would take place in a laser diffraction psd instrument, based on the actual geometry of the particles [46] and the internal geometry and nature of the detector of the instrument, extract what the equivalent spherical diameter would be, as measured by the instrument, then quantitatively analyze the results with the aid of the 3-D shape parameters of the particles analyzed.

It would be interesting to prepare a number of cements, each with differing mineralogy, and systematically grind them for various lengths of time and using varying kinds of grinders, with and without grinding aids. The shape could be characterized using the methods described in this paper, and then particle shape could be related quantitatively to these kinds of variables. Using standard shapes [10,11], unless they were randomly shaped, would not capture the details of cement powder. Even randomly-shaped standard shapes would need to be characterized by X-ray CT in the same way as was done for cement in this paper. Such a study could begin to lay the technical basis for cement manufacturers to have more control over particle shape. This data could then be related to early-age behavior such as hydration or rheology, which depends on particle shape (e.g. true specific surface area and cross-sectional area as a function of orientation).

## Acknowledgments

We would like to thank the Cement and Concrete Reference Laboratory for cement samples, and the members of the Virtual Cement and Concrete Testing Laboratory (VCCTL) for donation of samples and partial support of this work. We would also like to thank the National Synchrotron Light Source at Brookhaven National Laboratory, which is supported by the U.S. Department of Energy, Division of Materials Sciences and Division of Chemical Sciences, under Contract No. DE-AC02-98CH10886, for hosting us to do the X-ray CT measurements. We also thank Mr. Max Peltz for performing the laser diffraction measurements.

## References

[1] G. Polya, G. Szego, Isoperimetric Inequalities in Mathematical Physics, Princeton University Press, Princeton, 1951.
[2] J.F. Douglas, E.J. Garboczi, Intrinsic viscosity and polarizability of particles having a wide range of shapes, Adv. Chem. Phys. 91 (1995) 85–153.
[3] E.J. Garboczi, J.F. Douglas, Intrinsic conductivity of objects having arbitrary shape and conductivity, Phys. Rev., E 53 (1996) 6169–6180.
[4] M.L. Mansfield, J.F. Douglas, E.J. Garboczi, Intrinsic viscosity and the electrical polarizability of arbitrarily shaped objects, Phys. Rev., E 64 (2001) 61401–61416.
[5] ASTM Standard Test Method for Flat Particles, Elongated Particles, or Flat and Elongated Particles in Coarse Aggregate (D 4791-05), ASTM Vol. 4.03.
[6] J.W. Bullard, P.E. Stutzman, Analysis of CCRL proficiency cements 151 and 152 using the virtual cement and concrete testing laboratory (vol 8, pg 1548, 2006), Cem. Concr. Res. 37 (2007) 291–292; Cem. Concr. Res. 36 (2006) 1548–1555.

[7] A. Jillavenkatesa, S.J. Dapkunas, L.-S.H. Lum, NIST Recommended Practice Guide. Special Pubblication 960-1. Particle Size Characterization. 2001. National Institute of Standards and Technology, Department of Commerce, U.S. Government Printing Office. Available at: http://www.nist.gov/public_affairs/practiceguides/SP960-1.pdf.
[8] C.F. Ferraris, V.A. Hackley, A.I. Avilés, Measurement of particle size distribution in Portland cement powder: analysis of ASTM Round Robin Studies, Cem. Conc. Agg. 26 (2004) 71–81.
[9] T. Matsuyama, H. Yamamoto, B. Scarlett, Transformation of diffraction pattern due to ellipsoids into equivalent diameter distribution for spheres, Part. Part. Syst. Charact. 17 (2000) 41–46.
[10] R.N. Kelly, J. Kazanjian, Commercial reference shape standards use in the study of particle shape effect on laser diffraction particle size analysis, AAPS PharmSciTech 7 (2006) E1–E12 (Article 49).
[11] Richard N. Kelly, Kimberly J. DiSante, Elliott Stranzl, Jacqueline A. Kazanjian, Paul Bowen, Tatsuyama Matsuyama, Nadine Gabas, Graphical comparison of image analysis and laser diffraction particle, size analysis data obtained from the measurements of nonspherical particle systems, AAPS PharmSciTech 7 (3) (2006) E1–E14 (Article 69).
[12] C. Berthold, R. Klein, J. Luhmann, K.G. Nickel, Characterization of fibres and fibre collectives with common laser diffractometers, Part. Part. Syst. Charact. 17 (2000) 113–116.
[13] C. Berthold, W. Pabst, K.G. Nickel, Influence of detector geometries of common laser diffractometers on the particle size distribution of elongated particles, Fifth World Congress on Particle Technology (WCPT5), Orlando, USA, April 23–27 2006.
[14] N. Gabas, N. Hiquily, C. Laguérie, Response of laser diffraction particle sizer to anisometric particles, Part. Part. Syst. Charact. 11 (1994) 121–126.
[15] P. Bowen, J. Sheng, N. Jongen, Particle size distribution measurement of anisotropic particles cylinders and platelets — practical examples, Powder Technol. 128 (2002) 256–261.
[16] H. Mühlenweg, E.D. Hirleman, Laser diffraction spectroscopy: influence of particle shape and a shape adaptation technique, Part. Part. Syst. Charact. 15 (4) (1998) 163–169.
[17] S.T. Erdoğan, D.W. Fowler, E.J. Garboczi, Shape and size of microfine aggregates: X-ray microcomputed tomography vs. laser diffraction, Powder Technol. 177 (2007) 53–63.
[18] M.A. Taylor, E.J. Garboczi, S.T. Erdoğan, D.W. Fowler, Some properties of irregular particles in 3-D, Powder Technol. 162 (2006) 1–15.
[19] R.A. Ketcham, W.D. Carlson, Acquisition, optimization, and interpretation of X-ray computed tomographic imagery: applications to the geosciences, Comput. Geosci. 27 (2001) 381–400.
[20] S. Lu, E.N. Landis, D.T. Keane, X-ray microtomographic studies of pore structure and permeability in Portland cement concrete, Mater. Struct. 39 (2006) 611–620.
[21] N.N. Naik, A.C. Jupe, S.R. Stock, A.P. Wilkinson, P.L. Lee, K.E. Kurtis, Sulfate attack monitored by microCT and EDXRD: influence of cement type, water-to-cement ratio, and aggregate, Cem. Concr. Res. 36 (2006) 144–159.
[22] E. Gallucci, K. Scrivener, A. Groso, M. Stampanoni, G. Margaritondo, 3D experimental investigation of the microstructure of cement pastes using synchrotron X-ray microtomography, Cem. Concr. Res. 37 (2007) 360–368.
[23] D.P. Bentz, et al., The visible cement data set, J. Res. Natl. Inst. Stand. Technol. 107 (2002) 137–148.
[24] E.J. Garboczi, Three-dimensional mathematical analysis of particle shape using X-ray tomography and spherical harmonics: application to aggregates used in concrete, Cem. Concr. Res. 32 (2002) 1621–1638.
[25] S.T. Erdoğan, et al., Three-dimensional shape analysis of coarse aggregates: new techniques for and preliminary results on several different coarse aggregates and reference rocks, Cem. Concr. Res. 36 (2006) 1619–1627.
[26] M. El-Shenawee, E. Miller, Spherical harmonics microwave algorithm for shape and location reconstruction of breast cancer tumor, IEEE Trans. Med. Imag. 25 (2006) 1258–1271.
[27] E.J. Garboczi, J.W. Bullard, Shape analysis of a reference cement, Cem. Concr. Res. 34 (2004) 1933–1937.
[28] P.E. Stutzman, Multi-spectral imaging of cementitious materials, Proc. 29th Inter. Conf. on Cement Microscopy, Quebec City, Quebec, Canada, May 21–24 2007.
[29] D.P. Bentz, P.E. Stutzman, C.J. Haecker, S. Remond, H.S. Pietersen, J.A. Larbi, H.H.A. Janssen, SEM/X-ray imaging of cement-based materials, Proceedings of the 7th Euroseminar on Microscopy Applied to Building Materials, Delft Univ. Tech., 1999, pp. 457–466, Available at http://ciks.cbt.nist.gov/monograph, Part I, Ch. 3, Section 4a.
[30] L. Holzer, R.J. Flatt, S.T. Erdoğan, X. Nie, E.J. Garboczi, Shape comparison between 0.4 μm to 2.0 μm and 20 μm to 60 μm cement particles, J. Amer. Ceram. Soc. (in press).
[31] H.C. van de Hulst, Light Scattering by Small Particles, Dover, New York, 1981.
[32] G. Mie, Beiträge zur Optik trüber Medien, speziell kolloidaler Metallösungen, Ann. Phys. Leipzig 25 (1908) 377–445.
[33] O. Glatter, Determination of particle-size distribution functions from small-angle scattering data by means of the indirect transformation method, J. Appl. Crystallogr. 13 (1980) 7–11.
[34] Mohsen A. Khalili, Wayne L. Roricht, S.Y. Luke Lee, An Investigation to determine the precision for measuring particle size distribution by laser diffraction, World Congress on Particle Technology 4, Sydney 2002, Paper no 111.
[35] A.C. Kak, M. Slaney, Principles of Computerized Tomographic Imaging, SIAM, New York, 2001.
[36] J.H. Dunsmuir, X-ray Microtomography, Guidebook to Imaging and Microspectroscopy at the NSLS, May 2002, http://www.nsls.bnl.gov/newsroom/publications/otherpubs/imaging/workshopdunsmuir.pdf.
[37] M. Grigoriu, E.J. Garboczi, C. Kafali, Spherical harmonic-based random fields for aggregates used in concrete, Powder Technol. 166 (2006) 123–138.
[38] L.M. Hills, The Effect of Clinker Microstructure on Grindability: Literature Review Database, PCA Report 331, 1995.
[39] K. Velez, S. Maximilien, D. Damidot, G. Fantozzi, F. Sorrentino, Determination by nanoindentation of elastic modulus and hardness of pure constituents of Portland cement clinker, Cem. Concr. Res. 31 (2001) 555–561.
[40] Larnite crystal data, http://rruff.geo.arizona.edu/doclib/hom/larnite.pdf.
[41] K. Sommer, 40 years of presentation particle size distributions — yet still incorrect, Part. Part. Syst. Charact. 18 (2001) 22–25.
[42] S.T. Erdoğan, M.S. thesis, The effect of aggregates on the properties of concrete and proportioning methods, University of Texas at Austin, Austin, Texas, August, 2003.
[43] S.T. Erdoğan, Ph.D. thesis, Determination of aggregate shape properties using X-ray tomographic methods and the effect of shape on concrete rheology, University of Texas at Austin, Austin, Texas, 2005.
[44] J.M.R. Fernlund, The effect of particle form on sieve analysis: a test by image analysis, Eng. Geol. 50 (1998) 111–124.
[45] N.S. Martys, Study of a dissipative particle dynamics based approach for modeling suspensions, J. Rheol. 49 (2005) 401–424.
[46] M.I. Mishchenko, J.W. Hovenier, L.D. Travis (Eds.), Light Scattering by Non-Spherical Particles: Theory, Measurements, and Applications, Academic Press, San Diego, 2000.